JGR Biogeosciences

RESEARCH ARTICLE
10.1029/2023JG007465

# Surface Energy Dynamics and Canopy Structural Properties in Intact and Disturbed Forests in the Southern Amazon

**Ekena Rangel Pinagé[1,2], David M. Bell[3], Marcos Longo[4,5], Carlos A. Silva[6], Ovidiu Csillik[4], and Alfredo Huete[1]**

[1]School of Life Sciences, University of Technology Sydney, Ultimo, NSW, Australia, [2]College of Forestry, Oregon State University, Corvallis, OR, USA, [3]Pacific Northwest Research Station, USDA Forest Service, Corvallis, OR, USA, [4]Jet Propulsion Laboratory, California Institute of Technology, Pasadena, CA, USA, [5]Climate and Ecosystem Sciences Division, Lawrence Berkeley National Laboratory, Berkeley, CA, USA, [6]Forest Biometrics, Remote Sensing and Artificial Intelligence Laboratory, School of Forest, Fisheries and Geomatics Sciences, University of Florida, Gainesville, FL, USA

**Abstract** The Brazilian Amazon has been a focus of land development with large swaths of forests converted to agriculture. Forest degradation by selective logging and fires has accompanied the agricultural frontier and has resulted in significant impacts on Amazonian ecosystems. Changes in forest structure resulting from forest disturbances have large impacts on the surface energy balance, including on land surface temperature (LST) and evapotranspiration (ET). This study's objective is to assess the effects of forest disturbances on water fluxes and forest structure in a transitional forest site in the Southern Amazon. We used ET and LST products from MODIS and Landsat 8 and GEDI-derived forest structure data to address our research questions. We found that disturbances induced seasonal water stress, more pronounced in croplands/pastures than in forests (differences up to 20% in the dry season), and more pronounced in second-growth and recently burned areas than in logged and intact forests (differences up to 12% in the dry season). Moreover, ET and LST were negatively related, with more consistent relationships across disturbance classes in the dry season ($R^2$: 0.41–0.87) than in the wet season ($R^2$: 0.18–0.49). Forest and cropland or pasture classes showed contrasting relationships in the dry season. Finally, we found that forest structure exhibited stronger relationships with ET and LST in the most disturbed forests ($R^2$: 0.01–0.43) than in the least disturbed forests ($R^2 < 0.05$). Our findings help to elucidate degraded forests functioning under a changing climate and to improve estimates of water and energy fluxes in Amazonian degraded forests.

**Plain Language Summary** Deforestation, selective timber extraction, and forest fires are the main causes of forest disturbances in the Amazon region. These disturbances alter how forests function. Forest degraded by logging and fires may exchange less water and absorb less carbon dioxide from the atmosphere during photosynthesis. We used satellite-based observations on the amount of water transpired to the atmosphere by trees (known as evapotranspiration), land surface temperature, and forest structural properties such as canopy cover and height over a region in the Southern Amazon to understand the differences in function between disturbed and intact forests. We found that disturbances induced stronger and earlier water stress in the dry season in croplands and pastures than in forests, and stronger water stress in second growth and recently burned areas than in logged and intact forests. We also found that structural properties show a moderate relationship with evapotranspiration and temperature in the most disturbed forests, but weak relationships in the least disturbed forests. Our findings highlight the importance of intact forests in maintaining water balance in the Amazon region and suggest that disturbed forests may have limited ability to cope with the changing climate.

**Key Points:**

- Evapotranspiration (ET), surface temperature, and forest structure data can inform about the effects of canopy cover changes in the Amazon
- Forest disturbances affect ET-temperature relationships differently across wet and dry seasons and disturbance levels
- Forest structure exerts a stronger control on ET in the more disturbed/drier forests than in intact or lightly disturbed forests

**Supporting Information:**

Supporting Information may be found in the online version of this article.

**Correspondence to:**

E. R. Pinagé,
ekenapinage@hotmail.com

**Citation:**

Rangel Pinagé, E., Bell, D. M., Longo, M., Silva, C. A., Csillik, O., & Huete, A. (2023). Surface energy dynamics and canopy structural properties in intact and disturbed forests in the Southern Amazon. *Journal of Geophysical Research: Biogeosciences*, *128*, e2023JG007465. https://doi.org/10.1029/2023JG007465

Received 3 MAR 2023
Accepted 14 AUG 2023

**Author Contributions:**

**Conceptualization:** Ekena Rangel Pinagé, David M. Bell, Alfredo Huete
**Data curation:** Ekena Rangel Pinagé
**Formal analysis:** Ekena Rangel Pinagé, David M. Bell, Marcos Longo, Carlos A. Silva, Ovidiu Csillik
**Investigation:** Ekena Rangel Pinagé, David M. Bell
**Methodology:** Ekena Rangel Pinagé, David M. Bell, Marcos Longo, Alfredo Huete
**Resources:** Ekena Rangel Pinagé, Marcos Longo, Carlos A. Silva, Ovidiu Csillik



## 1. Introduction

Changes in tree cover and forest structure have large impacts on energy balance and ecosystem properties, altering components of the biosphere-atmosphere interactions that operate from the leaf (plant physiology) to global (atmospheric circulation) scales. Deforestation and forest degradation can alter rainfall regimes, water availability, and surface-atmosphere flux of water and energy of tropical forests (Davidson et al., 2012; Jucker et al., 2018; Longo et al., 2020; Spracklen et al., 2018). These impacts are particularly pronounced in ecotonal, semi-deciduous tropical forests of the southern Amazon Basin, which have experienced rapid regional warming and deforestation over the last three decades (Vourlitis et al., 2008). However, integrated assessments linking

**Software:** Ekena Rangel Pinagé
**Supervision:** David M. Bell, Alfredo Huete
**Visualization:** Ekena Rangel Pinagé
**Writing – original draft:** Ekena Rangel Pinagé
**Writing – review & editing:** Ekena Rangel Pinagé, David M. Bell, Marcos Longo, Carlos A. Silva, Ovidiu Csillik, Alfredo Huete

structural and functional changes resulting from forest disturbances are still lacking, and climate and forecast models are incipient in representing the influence of canopy structure on energy and water balances in degraded Amazon forests (Huang et al., 2020; Longo et al., 2020).

Chief among the water balance variables, evapotranspiration (ET) is a multi-faceted variable controlled by a combination of vegetation, atmospheric, and radiative drivers. ET measurements need to ensure that the abiotic and biotic controls are adequately captured: net radiation and land surface temperature (LST) provide the physical drivers for the state change of water and the subsequent impact on latent and sensible heat partitioning; humidity and air temperature regulate the transfer of water from the land into the air, and phenology and vegetation cover information are necessary for seasonal dynamics and relative magnitudes of ET fluxes (Fisher et al., 2008). One critical measurement to the estimation of remotely-sensed ET is the LST, as it can capture fine spatial and temporal dynamics associated with heterogeneous land surface processes controlling ET (Fisher et al., 2017).

Variability in the strength of ET drivers may be linked to different degrees of the canopy–atmosphere coupling (Jarvis & McNaughton, 1986). The control of ET can be viewed as complex supply-demand interactions, where net radiation and soil moisture represent the supply and the atmospheric vapor pressure deficit (VPD) represents the demand. This supply-demand interaction accelerates the biophysical feedback in ET. The degree of biophysical control is a function of the ratio of canopy conductance (an aggregated measure of canopy control on transpiration) to aerodynamic conductance. When the canopy and aerodynamic conductance ratio is very small (i.e., water-stress conditions), stomata principally control the water loss and a change in canopy conductance results in a nearly proportional change in transpiration. Such conditions trigger a strong biophysical control on transpiration. In this case, vegetation is believed to be fully coupled to the atmosphere. In contrast, for a high canopy and aerodynamic conductance ratio (i.e., high water availability), changes in canopy conductance will have little effect on the transpiration rate, and transpiration is predominantly controlled by net radiation (Mallick et al., 2016).

In the Amazon basin, ET exerts a large influence on regional and global climate patterns, and provides a significant source of rainfall water in South America (Maeda et al., 2017; Spracklen et al., 2012; van der Ent et al., 2010), by returning to the atmosphere between 50% and 75% of the regional precipitation (Lathuillière et al., 2012; Malhi et al., 2002). The major environmental controls driving spatial and temporal variability of ET in the Amazon are solar radiation (accounting for more than 80% of ET variability), atmospheric VPD, vegetation cover, and precipitation (Fisher et al., 2009), but complex interactions resulting from local climatic and biotic conditions generate highly heterogeneous patterns across the region (Fisher et al., 2009; Hasler & Avissar, 2007; Maeda et al., 2017). Synergies between climate and forest structure and functioning control much of the spatial variability in water and energy balances in the Amazon (Coe et al., 2016). While forest ET increases during the dry season in equatorial Amazonian forests, seasonally dry forests at the southern fringe of the biome present the opposite trend (da Rocha et al., 2009; Hasler & Avissar, 2007; Restrepo-Coupe et al., 2013).

Land cover changes alter vegetation cover and structure as well as land surface properties such as albedo, emissivity, and surface roughness (Bonan, 2008; Bright et al., 2015). Ultimately, the conversion of natural areas to urban or agricultural development affects gas and energy exchange processes between the land surface and the atmosphere, by changing how incoming precipitation and radiation are partitioned among sensible and latent heat fluxes and run-off (Coe et al., 2016). Decreased forest cover increases surface albedo and reduces net radiation and ET (Costa & Foley, 1997). Based on eddy covariance data collected in the Western Amazon, von Randow et al. (2004) found evapotranspiration rates 20%–41% lower in pastures compared to forests. Silvério et al. (2015) showed, for a large river basin in the southern Amazon, that abrupt transitions in land use such as forest/crops and forest/pastures decreased ET by 32% and 24%, respectively. These authors also found that LST was 6.4°C higher over croplands and 4.3°C higher over pasturelands, compared to the forests they replaced. Using an ecosystem demography model calibrated with tropical forest parameters, Longo et al. (2020) estimated that severely degraded forests experience water-stress with ET declines up to 34% and increases in daily mean ground temperatures (up to 6.5°C) relative to intact forests. Seasonality of water and energy fluxes also amplifies differences among disturbed and intact vegetation, due to their differential capability to access subsurface water during seasonal drought (von Randow et al., 2004; Zemp et al., 2017).

Disturbed forests in the Amazon are expected to transpire substantially less compared to old-growth forests, because of the potential reductions in leaf area index (LAI) and rooting depth (Silvério et al., 2015), but recent research has shown contrasting results. Some degraded forests have shown ET levels similar to intact forests' or

**Table 1**
*Hypotheses and Data Sets for the Research Questions*

| Research questions | Hypotheses tested | Data sets used |
|---|---|---|
| Q1. What is the effect of forest disturbances on the seasonal water stress of the canopy? | H1. Areas with decreased vegetative cover exhibit reduced ET earlier in the dry season, with equivalent water stress | MODIS MYD16A2 product (Total Evapotranspiration and Total Potential Evapotranspiration layers), 1 year of 8-day composites at 500-m resolution |
| Q2a. How are variations in seasonal water stress manifested in LST and ET relationships in the study site? | H2.a. LST is higher in areas with low ET and canopy cover | Landsat 8 LST, Landsat 8 ET (derived from the METRIC model), wet and dry season single dates at 30-m resolution |
| Q2b. Do these relationships vary with season and disturbance level? | H2.b. The negative ET-LST relationship will be stronger in more severely disturbed forests and during periods of greater water stress | |
| Q3. What is the contribution of canopy structural properties to ET? | H3. ET and LST covaries with structural properties in Amazon disturbed forests | Landsat 8 ET (derived from the METRIC model), dry season single date at 30-m resolution; Structural properties (canopy cover, plant area index, top-of-canopy height, and foliage height diversity) from GEDI at 25-m footprint |

even increased ET after a few years after fires or start of the secondary growth, with no corresponding recovery in structural attributes such as biomass or LAI (Brando et al., 2019; Von Randow et al., 2020). Canopy structural properties are intrinsically affected by disturbance type, intensity, and time since events. Given that changes in tree cover and structure have large impacts on energy balance and ecosystem properties, there is an urgent need to quantify these properties not only for mature forests but also for forests with lower, less complex cover and structure.

Active and optical remote sensing approaches have been widely used to directly observe or estimate LST, ET and forest structural properties. MODIS has long run and well-established ET products, but its coarse resolution may not be adequate to capture the ET variability associated with small-scale disturbances. Therefore, we also used ET derived from Landsat 8 data, retrieved as a residual of the surface energy balance (SEBAL algorithm; Bastiaanssen et al., 1998), using LST observations as the most important input. Landsat is the longest running continuous satellite program and is a finer-resolution alternative to MODIS. The most recent Landsat launches (8 and 9) show improved geometric and radiometric calibration compared to their 5 and 7 counterparts (Wulder et al., 2019). Laser scanning, an active form of remote sensing commonly known as lidar, is suitable to characterize three-dimensional forest structural properties (Lefsky et al., 2002). The Global Ecosystem Dynamics Investigation (GEDI) spaceborne lidar instrument has been providing unprecedented three-dimensional information of tropical and temperate forests worldwide (Dubayah et al., 2020, 2022; Duncanson et al., 2022) and has made it possible to investigate forest structure over large areas in the Amazon and other forest biomes worldwide.

The objective of this study is to assess the effects of forest disturbances (both deforestation/total canopy cover (CC) removal, and degradation/partial CC removal) on the seasonal ET fluxes and canopy structural properties in a transitional forest site located in Mato Grosso State, Southern Amazon. We use ET and LST data from MODIS and Landsat 8 OLI and TIRS sensors, taking advantage of their well-established record in the investigation of water fluxes (Anderson et al., 2012; Mu et al., 2011), as well as the novel GEDI forest structure data (Dubayah et al., 2022) to address the following questions: (a) What is the effect of forest disturbances on the seasonal water stress of the canopy? (b) How are variations in seasonal water stress manifested in LST-ET relationships across the study site, and do these relationships vary with season and disturbance severity levels? (c) What is the contribution of canopy structural properties to ET? Table 1 summarizes our research questions and related hypotheses, and the data sets used to address each of them.

## 2. Material and Methods

### 2.1. Study Area

The study area covers approximately 100,000 km$^2$ at the southern and drier flank of closed-canopy Amazon forests in the Brazilian state of Mato Grosso (Figure 1), including the municipality of Feliz Natal. The area is covered by evergreen broadleaf forests (IBGE, 2021). A 5-month dry season (May to September) accounts for only 6% of mean annual precipitation (inset in Figure 1).

This site is located in the "Arc of deforestation," a region that surrounds the southern edge of the Amazon biome, where conventional practices include land clearing for cattle ranching, small-scale subsistence farming, logging, and, increasingly, soybean production for global markets. Decades of agricultural expansion (which includes fire as a land clearing technique) and selective logging have left a mosaic of fragmented and degraded forests in the area (Matricardi et al., 2010; Morton et al., 2013; Souza et al., 2005), with the majority of intact forests remaining inside the indigenous reserves (Figure 1).

### 2.2. Disturbance History Assessment

We mapped the land cover/land use of the Feliz Natal region from 2000 to 2018, including both disturbances that lead to degradation of standing forests (selective logging and fires) and classes

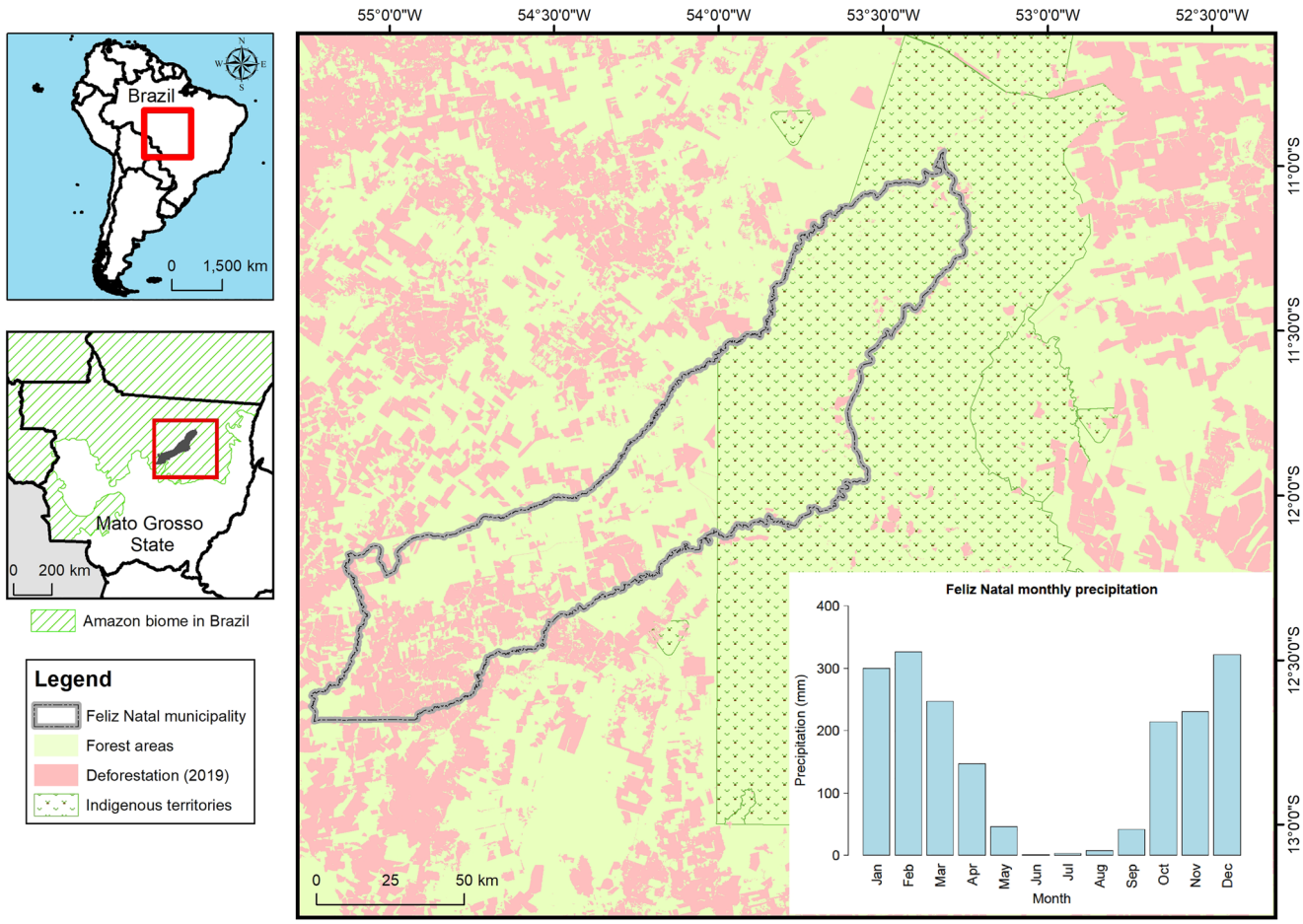


**Figure 1.** Location, forest cover and monthly precipitation (inset) of the study area. Source of precipitation data: climate-data.org. Source of deforestation data: INPE (2020).

of land use that follow stand-replacement disturbances (croplands, pastures and secondary forests). To map forest degradation, we masked out accumulated deforestation until 2019 (INPE, 2020) and areas of alluvial vegetation. Subsequently, we mapped logged and burned areas on the forest remnants based on visual interpretation of yearly fitted Normalized Burn Ratio images derived from Landsat 5, 7, and 8 observations. To differentiate forests experiencing variable degrees of disturbance, we classified degraded forests into six classes: 0–3 years (L1), 4–7 years (L2), and 8–14 (L3) years after logging, and 0–3 years (B1), 4–7 years (B2), and 8–14 (B3) years after burning, while forested areas with no signs of logging or fires in the time-series were classified as intact forests (IN). Polygons that experienced multiple degradation events in the time-series were classified according to the latest event. Details of the methodology for mapping intact and degraded forests can be found in Rangel Pinagé et al. (2022).

Subsequently, we included classes of land cover following deforestation in the disturbance history. Crop (CR) and pasture (PA) polygons for 2019 were obtained from the MapBiomas Collection 5 data of Brazil's annual land cover and use maps, based on Landsat images (MapBiomas Project, 2019). Also from MapBiomas data, we extracted a land cover class representing the transition of pasture and crops to forest cover from 2015 to 2019 to represent young secondary forests (SFN). Next, we extracted data for the old secondary forest class (SFO) from the TerraClass data set, which classifies land uses following deforestation in the Amazon, based on Landsat and MODIS data. We chose to use TerraClass until 2014 instead of the regeneration data from MapBiomas because the former is more consistent with the INPE methodology for deforestation mapping (Almeida et al., 2016).

The consolidated layer of disturbance history was generated by merging the forest degradation, old secondary forest (from TerraClass), and crop/pasture and young secondary forest (from MapBiomas) individual layers (Figure 2). We eliminated isolated polygons with areas smaller than 50 ha to be consistent with MODIS resolution.

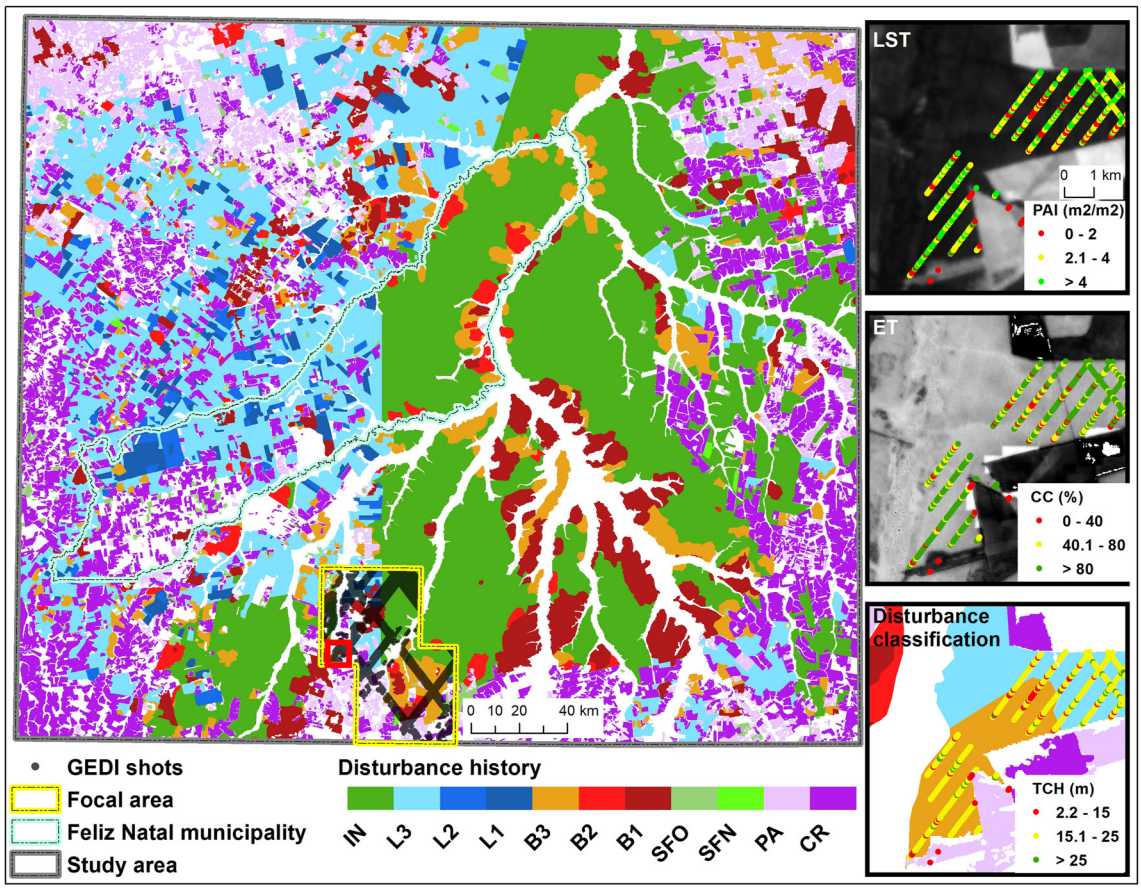


**Figure 2.** Disturbance classification at Feliz Natal region and post-filtered Global Ecosystem Dynamics Investigation (GEDI) shots over the focal area (yellow outline polygon). Insets are zooms from the red outline polygon in the main map and show GEDI structural properties (plant area index (PAI), canopy cover (CC), and top-of-canopy height (TCH)). Inset background images are land surface temperature (LST) and evapotranspiration (ET) from September 2019. Higher values of LST and ET are brighter. Unclassified areas (over alluvial vegetation or savannas, or due to a mismatch among input data sets) are shown in white in the disturbance classification.

### 2.3. Remote Sensing Data

The remote sensing data employed in this study includes ET modeled from MODIS observations, ET (modeled) and LST from Landsat 8 observations, and forest structural properties from GEDI observations.

#### 2.3.1. MODIS Data

Due to its high temporal resolution and compositing scheme, MODIS data allow for the generation of consistent seasonal patterns. To address Q1, we used the MYD16A2 Version 6 Evapotranspiration/Latent Heat Flux product, an 8-day composite data set produced at 500-m resolution (Running et al., 2017). The layers ET_500m (for total evapotranspiration) and PET_500m (for total potential evapotranspiration) were selected, along with the quality control flag layer to filter out low-quality data. The improved algorithm of product MYD16A2 is based on the logic of the Penman-Monteith equation, which includes inputs of daily meteorological reanalysis data along with MODIS data products such as vegetation property dynamics, albedo, and land cover. The pixel values for the ET and PET layers represent the sum of all 8 days within the composite period.

To test the hypothesis that areas with low forest cover experience water stress earlier in the dry season (H1), we applied the concept of Evaporative Stress Index (ESI; Fisher, 2013), computed from the ratio between actual and potential evapotranspiration. Any ET less than the PET is an indicator that water supply is limited; plants may close stomata to conserve water, and productivity may therefore be less than optimal. Hence, the actual-to-potential ET ratio (ET/PET) is a key indicator of plant water stress (low values of ESI are associated with increased water stress, and high ESI values are associated with lack of water stress). Moreover, anomalies to ET/PET can provide

valuable information about water stress without requiring precipitation or soil moisture information (Anderson et al., 2012). We divided the ET by the PET layer, extracted the pixels over the polygons of each disturbance class, and finally, extracted their mean values for each 8-day composite to build the 2019 annual profile of ESI.

#### 2.3.2. Landsat 8 OLI and TIRS Data

While MODIS ET estimates are valuable for understanding spatially integrated regional ET patterns and seasonality, they are not able to capture fine-scale spatial dynamics associated with heterogeneous land surface processes controlling ET. Hence, to address Q2 and Q3, which are related to relationships of ET with LST and forest structure, we used Landsat data at 30-m resolution over a ∼300,000-ha subset (approximately 3.5% of the total area, yellow outline polygon in Figure 2) within the same image scene. Using one single scene minimizes inconsistency of ET values across disturbance classes. For Q2, we compared ET and LST relationships across disturbance classes at single dates at the wet (31 January 2019) and dry (28 September 2019) seasons. For Q3, we used the ET and LST data from September only along with structural variables from GEDI (described in the next section). We used only one dry season date to compare ET and LST relationships with forest structure data because the latter is not expected to change seasonally or daily, unlike process variables such as evapotranspiration or gross primary productivity.

LST and ET data were derived from Landsat 8 observations. The images were obtained through the Earth Engine Evapotranspiration Flux (EEFlux version 0.20.3, described by Allen et al. (2015)). EEFlux is based on the Mapping Evapotranspiration at High Resolution Internalized Calibration (METRIC) (Allen et al., 2007). Within EEFlux workflow, LST data is generated using a fixed atmospheric calibration, where the near-surface temperature gradients are an indexed function of radiometric surface temperature, thereby eliminating the need for absolutely accurate surface temperature and the need for air-temperature measurements. Actual evapotranspiration is derived from the Landsat images representing the 24-hr actual ET, via the standard automated calibration within EEFlux. In this framework, actual ET is calculated as a residual of the surface energy balance, according to the following equation:

$$\mathrm{LE} = R_n - H - \mathrm{G}$$

where LE is the latent heat flux (energy spent in the evapotranspiration process (W $m^{-2}$); $R_n$ is net radiation (W $m^{-2}$); $G$ is the heat flux in the soil (W $m^{-2}$), and $H$ is the sensible heat flux (W $m^{-2}$). The EEFlux calibration uses the Landsat thermal band and shortwave bands to estimate the surface energy balance and to estimate the amount of vegetation, albedo and surface roughness. Version 0.20.3 of EEFlux employs automated image calibration by assigning values for EToF (which represents ET as a fraction of the reference evapotranspiration) for the 'hot' and 'cold' pixels of the surface temperature spectrum of the scene. LE is estimated at the exact moment of the passage of the satellite for each pixel and instantaneous ET is then calculated by dividing the LE by the latent heat of vaporization, according to the following equation:

$$\mathrm{ET}_{\mathrm{inst}} = 3,600\mathrm{LE}/\lambda\rho w$$

where $\mathrm{ET}_{\mathrm{inst}}$ is the instant evapotranspiration (mm $h^{-1}$); 3,600 converts seconds to hours; $\lambda$ is the latent heat of vaporization (J $kg^{-1}$), and $\rho w$ is the density of water (∼1,000 $kg^{-3}$). Numata et al. (2017) assessed the accuracy of METRIC ET estimates for the Amazon region and found good agreement between METRIC and flux tower-derived ET ($R^2 > 0.7$).

To assess the ability of Landsat data to capture the seasonal water stress detected with MODIS, we chose two Landsat images of a subset of the study area (yellow polygon in Figure 2) from the wet and late dry seasons with the least cloud coverage and extracted the equivalent of an ESI (ratio of actual and reference ET).

#### 2.3.3. GEDI Data

GEDI produces high resolution 3D observations of Earth's forests and topography (Dubayah et al., 2020). GEDI's precise measurements of forest canopy height, canopy vertical structure, and surface elevation at a 25-m footprint can characterize important carbon and water cycling processes, biodiversity, and habitat (Dubayah et al., 2020).

To address Q3, we extracted four structural properties from GEDI Level 2A and 2B data: top of canopy height (TCH, m), plant area index (PAI, $m^2/m^2$), CC (%) and foliage height diversity (FHD, unitless). TCH was derived from level 2A data (GEDI L2A Canopy Elevation and Height Metrics). The RH98 (the 98th percentile return

height) was used as a proxy for TCH. PAI, CC, and FHD were derived from Level 2B (GEDI L2B Footprint CC and Vertical Profile Metrics) (Tang & Armston, 2019).

We processed the version 2 of GEDI Level 2A and Level 2B data for the study area, for the period between 5 May and 11 November 2019. To filter low-quality data, we only kept laser shots with the recommended quality flags (i.e., sensitivity ≥0.95, quality flag = 0, and degrade ≠ 0; Hofton et al., 2019). We used an additional filter to remove data in the adjacency of low-quality data, by keeping the shots along a single beam that were part of a continuous strike of at least 30 good quality filtered shots (Csillik et al., 2022). Finally, we excluded additional shots within fire scars detected in 2019 according to the DETER-B data sets (Diniz et al., 2015) and without associated values of ET or LST (i.e., due to cloud on Landsat observations). After the application of all filters, a total of 12.551 shots from the subset of the study area were retained (Figure 2). GEDI data processing was performed in a Geographic Information System platform and the *R* statistical software (R Core Team, 2021), with the aid of the rGEDI package (Silva et al., 2020).

### 2.4. Statistical Analysis

To compare ET and LST among the disturbance classes and across seasons, we applied the Tukey's Honestly Significant Difference test (henceforth Tukey's test) (Tukey, 1977) to identify statistically distinct groups.

To assess ET-LST relationships, we developed linear regression models with ET as the dependent variable. The models were fitted at the pixel level for dry and wet seasons for the disturbance classes separately. We did not fit models for the data encompassing all classes because the ET-LST relationship in that case was clearly nonlinear. In addition, we tested the differences in slope coefficients between wet and dry seasons for each group to evaluate how seasonal moisture stress influences the relationship between ET and LST. To minimize the effects of spatial autocorrelation, only 1 out of every 500 pixels were randomly selected and included in the regression models. Observations falling below the 2.5th and above the 97.5th percentiles were excluded, to minimize outliers that are likely to occur in the edges of polygons from the different classes.

To compare GEDI-derived structural properties among the disturbance classes, we also used violin plots and the Tukey's test to compare all possible pairs of means. Next, we fitted linear regression models at the GEDI footprint level with ET and LST as dependent variables and each structural attribute as the independent variable, to assess the relationship between ET or LST with structural variables. We made no assumptions on the normality or transformation of the data due the large sample size (>1,000 observations). All statistical tests, analysis and plotting were performed in the *R* statistical environment (R Core Team, 2021).

## 3. Results

### 3.1. Seasonal Water Stress

The 2019 annual profile of the ESI showed that forest and non-forest classes in Feliz Natal region experience year-round ESI <1(Figure 3). The disturbance classes showed varied evaporative stress in the dry season (May through September) and could be distinguished into two groups with well-marked water stress signals: croplands and pastures and forests (Figure 3).

Croplands and pastures exhibited the sharpest ESI decline at the onset of the dry season, with ESI almost reaching zero (meaning maximum evaporative stress or no vegetation cover) at the end of the dry season (Figure 3a). Pastures showed a similar annual pattern to that of croplands but with a less pronounced ESI decrease.

Evaporative Stress Index from the different forest classes declined sharply later in the dry season, with a less pronounced drop than crops and pastures. Among the forest classes, logged forests showed higher ESI than intact forests at the time of the most severe water stress signal in early September (0.45–0.46 and 0.39, respectively). Recently burned forests showed lower ESI than intact forests (0.36), whereas the older burned classes showed similar or higher ESI compared to intact forests (0.39–0.41). Meanwhile secondary forests showed slightly lower ESI values compared to the other forest classes (~0.33). Interestingly, pastures and croplands showed similar MODIS-based ESI levels as that of forests during most of the wet season (Figure 3a).

Water stress in the late dry season (in September) is also detected by Landsat data (Figure 3b), but with improved water stress discrimination among classes (e.g., larger differences within burned and secondary forests). However,

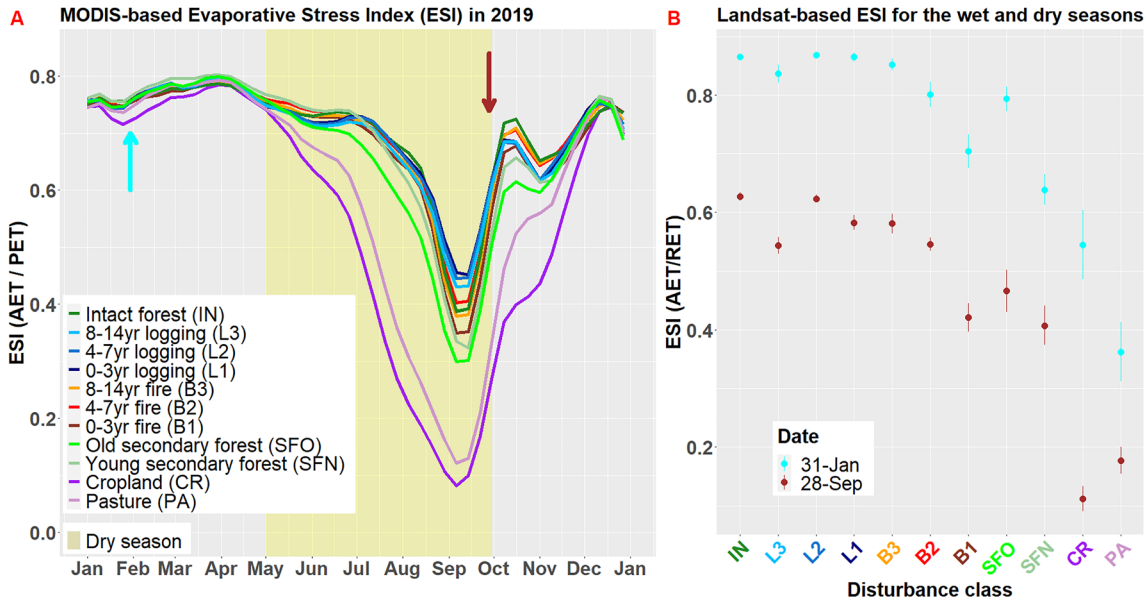


**Figure 3.** Annual profile of the MODIS Evaporative Stress Index (ESI) for the disturbance classes for Feliz Natal region (a). The cyan and brown arrows in A indicate the dates that the Landsat-based ESI for a subset of the study area was extracted (b). A sample of 100 Landsat pixels was included for each class. The error bars in B represent 95% confidence interval of the mean. Labels in the *x*-axis in B represent the disturbance classes and are in the same order and color of the legend in (a). Figure S1 in Supporting Information S1 shows the curves per disturbance class with the 95% range (1.96 standard deviation) confidence bands along the lines.

Landsat data showed larger differences between the least and most disturbed classes in both seasons with substantially lower ESI values for croplands and pastures, while MODIS ESI showed little divergence in the wet season (Figure 3a). Landsat's finer spatial resolution is likely producing this better discrimination, but it also could be due to different sensor characteristics and ET retrieval algorithms.

### 3.2. ET-LST Relationships

By using Landsat observations of LST and ET, we found that some croplands and pastures show moderate ET in January (wet season), comparable to degraded forests, and that ET differences within degraded and intact forests are amplified in September (dry season). LST on the other hand shows higher values in croplands and pastures in both analyzed periods, but with notably higher differences compared to forests in the dry season (Figure 4).

The seasonal variation in ET and LST was largely consistent with the continuum of disturbance intensity (Figure 5, sorted from intact forests to crops). ET and LST were inversely correlated, showing opposite trends in both wet and dry season dates. In January, most forest classes showed similarly high ET ranges (median: 3.4–3.8), except for the most recent burned and secondary forests (median: 3.2 and 2.9, respectively) (Figure 5a). Croplands and pastures showed greater variability than forests in January, but croplands exhibited a high proportion of pixels with high ET as well (median: 2.6 and 1.3, respectively). Toward the end of the dry season (e.g., September), following maximum evaporative stress (Figure 3), ET and LST in pasture and croplands were significantly different from all forest classes. Forests also showed increased ET and LST contrasts in the dry period compared to the wet season (Figure 5). LST showed a similar pattern of differentiation among the classes, but an opposite trend of values (higher in those classes with lower ET estimates, Figure 5b).

We found a strong negative relationship between ET and LST across disturbance classes, with a global correlation coefficient of −0.81 (Figure 6). Two clusters of points were observed in the dry season data: forest classes at one end (with intact forests at the edge of this cluster), and crops and pastures at the other end. In the wet season data, there is no such clear differentiation: ET from croplands and pastures shows greater variability, with the highest values in the same range of ET from forest classes. Moreover, the secondary forest classes mostly had their points spread in the transition between the two clusters in the dry season.

To assess ET and LST relationships over different land cover types, we merged the disturbance classes into five broad classes, namely intact, logged, burned and secondary forests, and croplands and pastures (Figure 6b). All

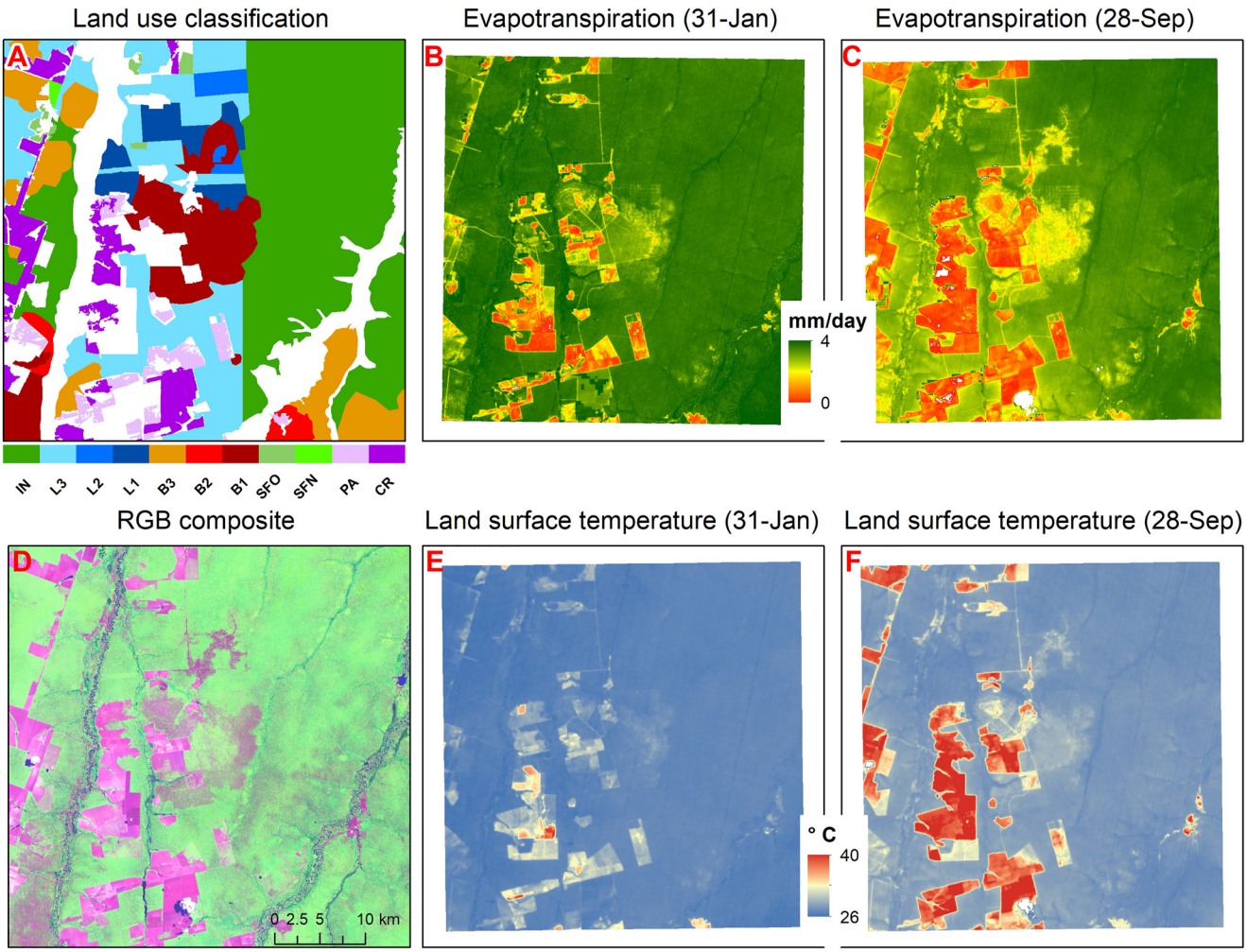


**Figure 4.** Disturbance classification (a), evapotranspiration in wet and dry seasons (b and c), a false-color RGB composite (d), and land surface temperature (LST) in wet and dry seasons (e and f) over a subset of the study area. RGB composite image info: Landsat 8, path/row 225/069, date 28 September 2019, R6G4B5. ET and LST data are from EEFlux.

the regression models were significant, but the regression coefficients varied widely. Dry season conditions strengthened ET-LST relationship (i.e., increased the coefficient of determination, $R^2$) in intact, logged, burned and secondary forests. Nevertheless, in terms of sensitivity of the relationship (i.e., the slope coefficient), burned and secondary forest classes showed very small or not significant differences in slope across seasons (Table 2). Croplands and pastures were the only class that showed a lower coefficient of determination, and a much lower slope in the dry season.

All classes showed significantly different slopes between wet and dry seasons ($p$-value $< 0.05$), except secondary forests ($p$-value $= 0.72$), whereas the largest difference was observed at the cropland and pasture class (Table 2). A significant finding is that intact and logged forests showed a positive difference in trend (significantly higher slope in the dry season), whereas burned and secondary forests showed a negative trend (implying smaller slopes in the dry season, but with non-significant or marginally significant differences).

### 3.3. Structure-Function Relationships

Forest structural properties derived from GEDI observations over our disturbance classes were significantly affected by disturbances. Classes following deforestation (secondary forests, croplands, and pastures) showed the most pronounced responses in the structural properties assessed (Figure 7). For both CC and PAI, intact forests showed the highest values, crops and pastures showed the lowest values and the least dispersed range,

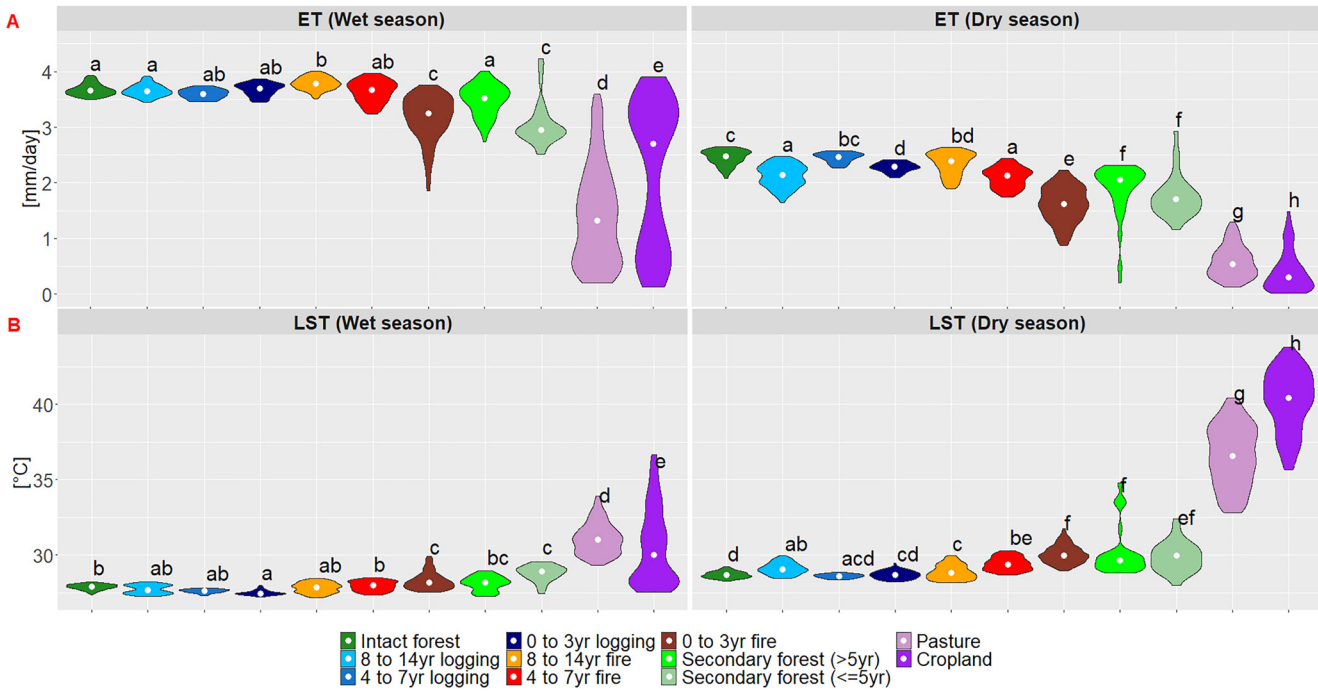


**Figure 5.** Distribution of ET (a) and land surface temperature (b) in the wet and dry seasons across the disturbance classes. Only 1/500 pixels were included, and observations falling below the 2.5th and above the 97.5th percentiles were excluded. Violin plots show the kernel probability density of the data at different values. All violins have the same width, and the median of each group is indicated by the white dots. Groups labeled with the same letter are not significantly different at a confidence level of 95% (Tukey's HSD test). The wet season image date is 31 January 2019, and the dry season image date is 28 September 2019.

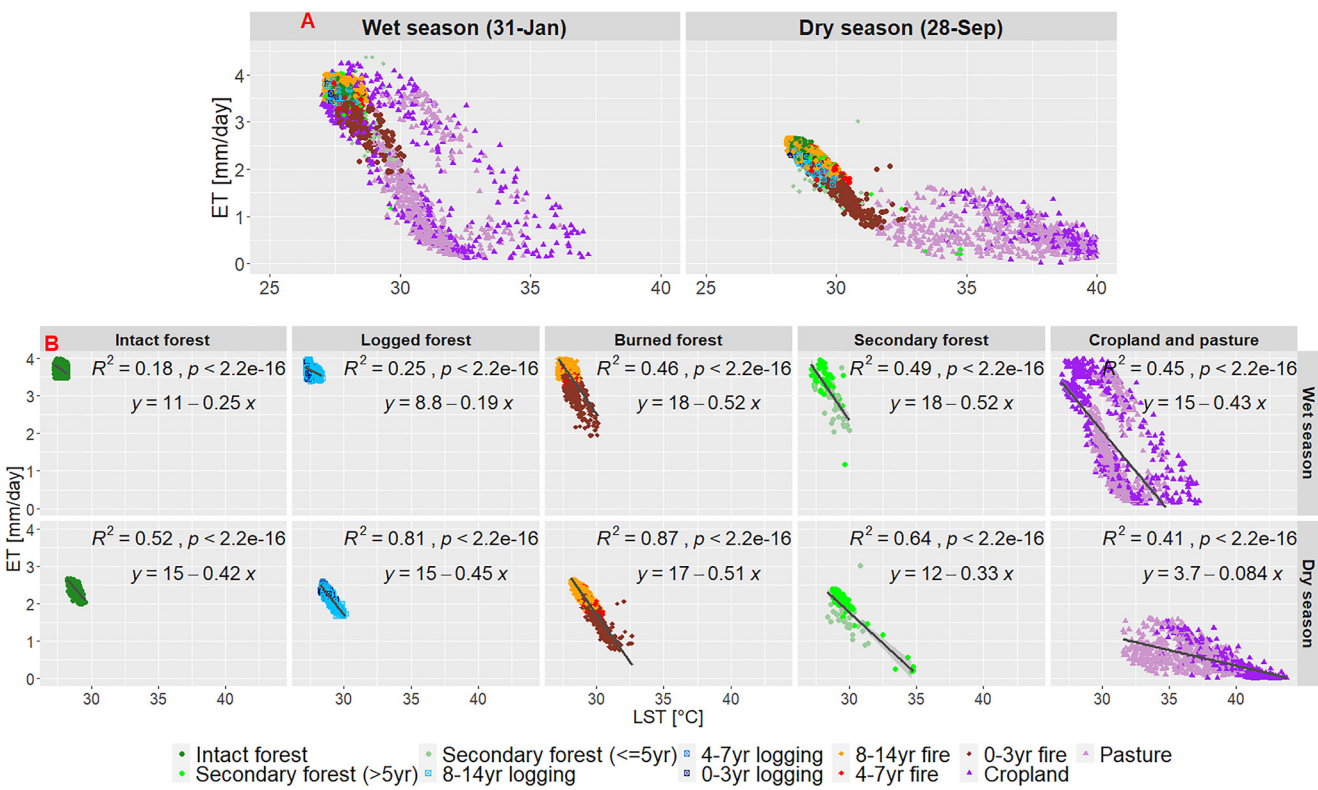


**Figure 6.** Relationship between ET and land surface temperature in wet and dry seasons for all classes (a), and for the broad disturbance classes separately (b). 1/500 pixels were randomly included, and observations falling below the 2.5th and above the 97.5th percentiles were excluded. Black lines represent the best fit line.

**Table 2**
*Estimates of Slope Differences Between Wet and Dry Season in ET and Land Surface Temperature Relationship for the Broad Disturbance Classes*

| Pair | Difference in trend | SE | *p*.value |
|---|---|---|---|
| Intact forest | 0.149 | 0.0182 | <0.0001 |
| Logged forest | 0.282 | 0.0149 | <0.0001 |
| Burned forest | −0.041 | 0.0133 | 0.002 |
| Secondary forest | −0.025 | 0.0710 | 0.720 |
| Croplands and pastures | −0.350 | 0.0138 | <0.0001 |

*Note.* *P*-values of pairwise comparisons >0.05 (highlighted in gray) indicate non-statistically significant differences in slope at 95% confidence level. SE stands for standard error.

whereas young secondary forests showed intermediate values and the broadest range. Burned and logged forests clearly responded to time since disturbance and disturbance type, as indicated by increasing CC and PAI with time since disturbance. Young secondary forests (≤5 years) showed CC and PAI similar to the most recent burns. FHD, a measure of structural complexity, showed very little variability among intact and logged forests, whereas burned and secondary forests and crops/pastures differed significantly from those classes. Except for the FHD metric, young secondary forests had all GEDI structural metrics not significantly different from crops and pastures.

To assess the relationships between structural properties and ET and LST, we grouped the disturbance classes into four broad categories: intact, logged, burned and secondary forests. Croplands and pastures were excluded from this analysis because the structure in these classes might be ephemeral (i.e., crops are harvested), making the examination of relationships of structure to ET and LST less meaningful.

Structural properties showed moderate to high correlations with ET (positively correlated, coefficients from 0.50 to 0.59) and LST (negatively correlated, coefficients from −0.50 to −0.76) (Table 3). The strongest relationships between structure and ET and LST were observed in the most intensively disturbed classes (burned and secondary forests), whereas intact and logged forests showed no significant slopes in the relationships. For instance, CC explained 43% and 25% of ET and LST in burned forests, and PAI explained 25%–30% of ET in burned and secondary forests. The greater regression slope for burned and secondary forests compared to intact and logged forests was consistent across all GEDI-derived structural properties (Figure 8).

ET and LST varied substantially among classes at the lower end of forest structure (short or low PAI forests), but not at the upper end (tall or high PAI forests) (Figure 8). There was a separation across the classes because intact and logged forests do not have extremely low PAI, CC, canopy height, and FHD values. Interestingly, ET and LST have different ranges between intact and logged versus secondary and burned forests with similar PAI or CC at the intermediate values. Moreover, the regression analysis suggests that most variation in ecosystem function (ET

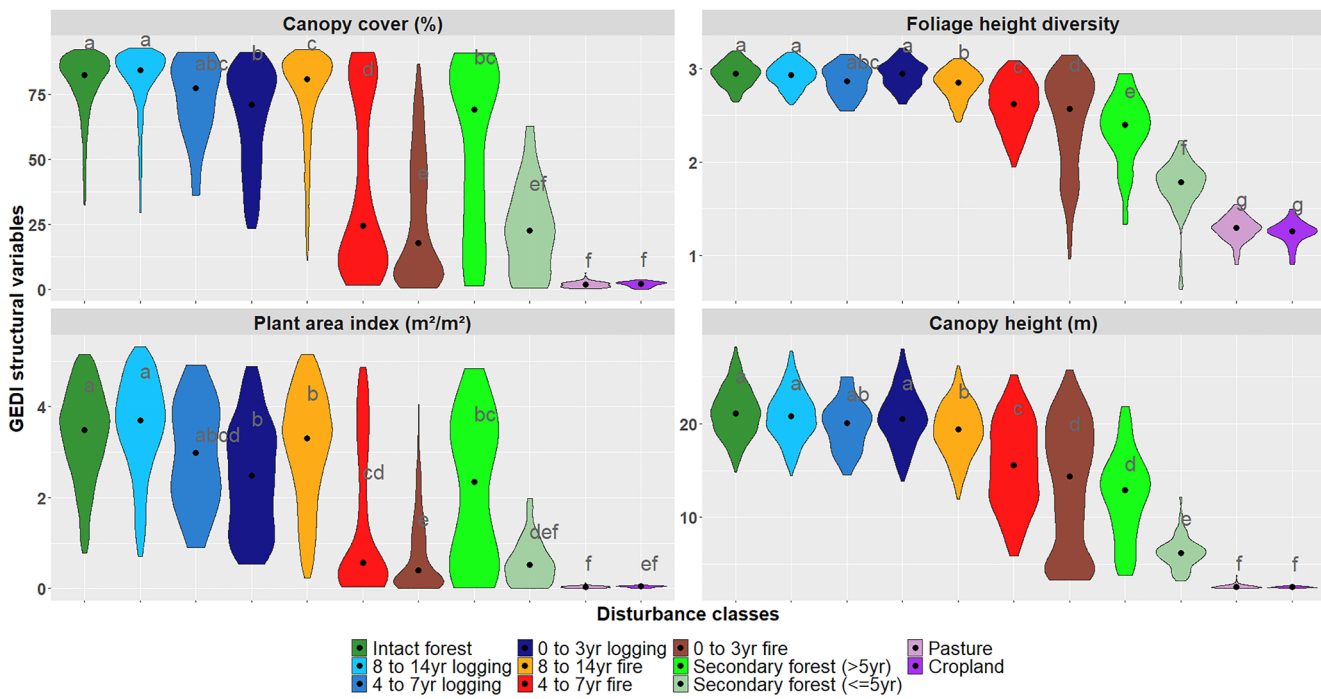


**Figure 7.** Structural properties derived from Global Ecosystem Dynamics Investigation data for the disturbance classes. Groups labeled with the same letter are not significantly different at a confidence level of 95% (Tukey's HSD test). Observations falling below the 2.5th and above the 97.5$_{th}$ percentiles were excluded.

**Table 3**
*Correlation Matrix of Structural Properties With Evapotranspiration (ET) and Land Surface Temperature (LST)*

| | Canopy height | Canopy cover | PAI | FHD | ET | LST |
|---|---|---|---|---|---|---|
| Canopy height | 1.00 | 0.79 | 0.71 | 0.93 | 0.56 | −0.67 |
| Canopy cover | | 1.00 | 0.95 | 0.74 | 0.59 | −0.62 |
| PAI | | | 1.00 | 0.63 | 0.50 | −0.50 |
| FHD | | | | 1.00 | 0.58 | −0.76 |
| ET | | | | | 1.00 | −0.77 |
| LST | | | | | | 1.00 |

*Note.* All correlations are significant at 99% confidence. Positive coefficients are shown in blue and negative coefficients are shown in red.

and LST) from these heavily disturbed forests can be explained by structure, whereas there is much lower variation in the least disturbed forests explained by structure and disturbance.

## 4. Discussion

In this study, we employed a novel combination of MODIS, Landsat, and GEDI observations to compare seasonal water stress and ET-LST relationships over a continuum of disturbance conditions; and to quantify the contribution of forest structure properties to ET and LST variability in secondary, degraded and intact forests. The results showed that disturbances increased seasonal water stress, earlier and more pronounced in croplands and pastures than in forests, and more pronounced in second-growth and recently burned areas than in logged and intact forests. Moreover, we found that the negative ET- LST relationships were more consistent across disturbance classes in the dry season, and that the forest and cropland/pasture classes showed contrasting relationships in the dry season. Finally, we found that structural properties of the canopy such as PAI, CC, canopy height, and FHD exhibited moderate relationships with ET and LST in the most disturbed forests, but negligible correlations in the least disturbed forests.

While we acknowledge some circularity of ET and LST being related to forest structure as per the MODIS ET algorithm (Running et al., 2019), we used independent forest structure data from GEDI, which are more direct measures than those derived from optical observations. Moreover, we found that the effect of forest structure on ET is spatially heterogeneous, with the strongest effects found in the more disturbed/drier forests. We consider this a key finding and contribution of this study.

### 4.1. Water Stress, ET and Land Surface Temperature Variability Across a Disturbance Continuum

The ESI seasonal profile analysis indicated that, while forest classes still showed some divergence in water stress especially at the end of the dry season, pastures and croplands in our study region are highly seasonal with a

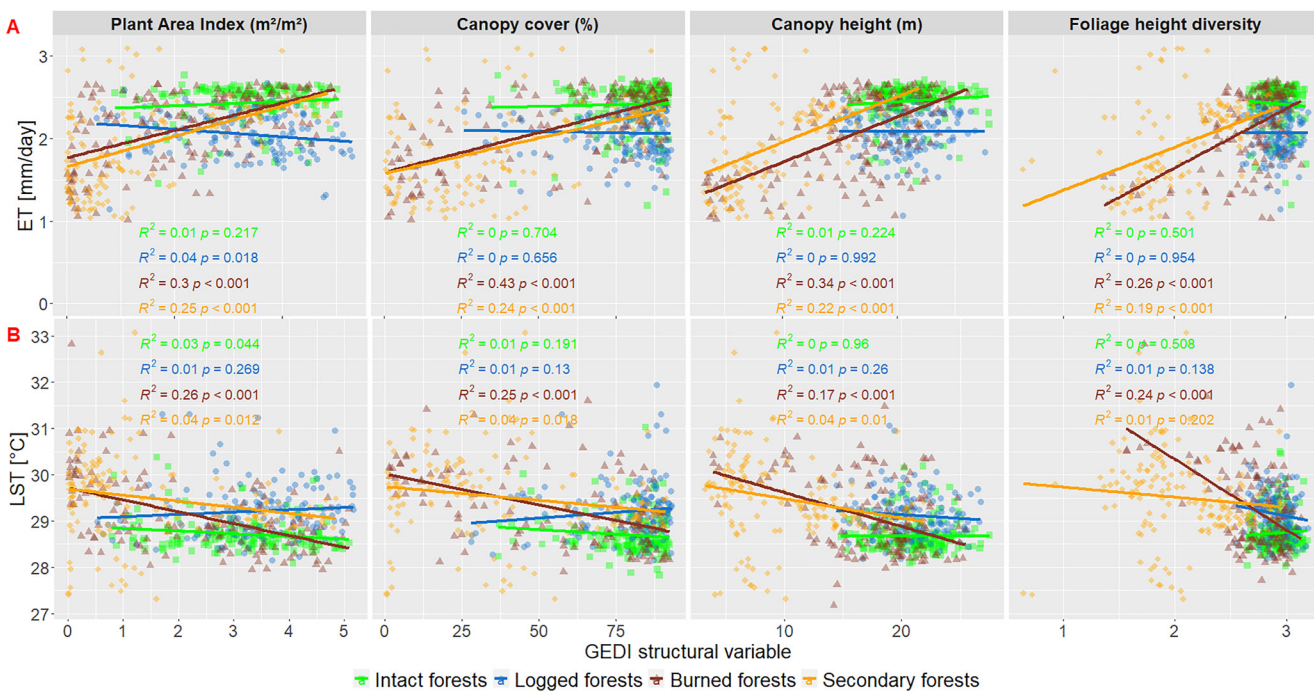


**Figure 8.** Relationship between Global Ecosystem Dynamics Investigation structural properties and evapotranspiration (a) and land surface temperature (b) for the broad forest classes. Lines represent the best fit from the linear regression models.

growing season-dependent exclusively on rainfall (Arvor et al., 2014) (Figure 3). This contrasting pattern occurs because the maximum rooting depth of these crops and grasses is far shallower than those of forests (Nepstad et al., 1994; O'Connor et al., 2019). But certainly, the most novel results of our study are those related to the behavior of secondary-growth and burned forests, showing that they experienced moderate and delayed water stress compared to intact and logged forests, related to changes in structural properties of these forests caused by disturbances (assessed with GEDI data) and potentially to species composition shifts (not assessed in this study).

ET generally increased and LST generally increased in the disturbance classes along a disturbance intensity continuum (intact forests < logged forests < burned forests < secondary forests < croplands and pastures). Although studies assessing ET and LST relationships in tropical forests are rare, the dry season declines in ET and increases in LST observed in this study (Figures 5 and 6) agree with similar comparisons in the southern Amazon. Hasler and Avissar (2007) found 5%–10% decreases in flux tower-measured ET in the dry season at sites in Rondônia and Mato Grosso States, while von Randow et al. (2004) found 25% less ET in pastures in Rondônia state during the dry season. In general, we found similar trends, but more pronounced ET declines from January to September (33%–40% at intact and least disturbed sites, and even greater declines (∼50%) for the most heavily degraded forests, with crops and pastures showing the largest differences (60%–80%), and greatest variability (Figures 4–6). These differences in magnitude could be due to the different methods of data acquisition (e.g., flux tower data vs. satellite-based estimates, or single flux tower sites vs. patch averages within a large area). Other plausible explanation for these differences is that the aforementioned studies used data from the early 2000's, while we looked at data from 2019. Temperatures and VPD increased in this interval, which could be adding more stress to these forests (Barkhordarian et al., 2019; Da Silva et al., 2019).

Despite slightly reduced PAI (Figure 7), the least disturbed forests such as logged and oldest burns showed ET and LST comparable to intact forests during both seasons (Figure 5), suggesting that albedo and net radiation on these forests recovered or never shifted from that of intact forests. Classes with intermediate levels of disturbance (4–7 yr fires and old secondary forests) showed stronger ET depletion during the dry season, and the most heavily degraded classes (0–3yr fire and young secondary forests) exhibited significantly lower LST and ET compared to intact forests on both seasons. These results agree with Miller et al. (2011), that found modest and ephemeral effects on the water and heat fluxes in a logged forest site in Central Amazon, with changes due to logging smaller than the interseasonal and interannual variability; these authors also found albedo not being significantly affected by logging activities. Similar to our results for burned forests, Brando et al. (2019) found that ET had fully recovered 7 years after experimental fires in the same region. Comparing ET between intact and 20-years old secondary forests in Central Amazon, Von Randow et al. (2020) found that secondary forests showed ET approximately 20% higher than primary forests over wet and dry seasons. Given the shorter and less severe dry season in Central Amazon compared to Feliz Natal region, it is reasonable to expect lower ET in the dry season in Feliz Natal. Moreover, our samples include a much larger spatial variability of secondary forest conditions.

The strongest (negative) ET-LST relationships were observed at the disturbance classes with larger ranges of ET and LST values (e.g., burned and secondary forests), rather than at the most severely disturbed classes (e.g., crops and pastures, Figure 6). Among the forest classes, variations in seasonal water stress manifested in ET-LST relationships in different ways: burned and secondary forests showed little change from wet to dry season (differences in trend from −0.04 to −0.02), whereas the dry season substantially improved ET-LST relationships at intact and logged forests (differences in trend from 0.15 to 0.28; Figure 6, Table 2). These findings, along with the ESI profile from Landsat (Figure 3b), suggest that patches of burned and secondary forests, especially the most recent ones, experience year-round moisture stress (e.g., patches with low ET and high LST even in the wet season). Therefore, strong inverse correlations between ET and LST in wet periods could be used as an indicator of water stress and inform about the functioning of disturbed forests.

Patchy mosaics are prominent following fires and can include severely disturbed patches adjacent to fragments with substantial residual vegetation and organic matter (Chazdon, 2003). In this sense, Landsat ET and LST estimates showed improved discrimination of the internal ET and LST variability of these patches. While MODIS data showed similarly low water stress across all forest classes in January (Figure 3a), Landsat finer-scale data showed larger differences among those classes even in the wet season (Figure 3b). These larger differences in the Landsat-based ESI imply that MODIS-based assessments of water fluxes or water-use efficiency (e.g., Brunsell et al., 2020) may be underestimating moisture deficit in these more degraded and patchier areas such as burned forests.

Taken together, these results highlight the wide range of forest functional responses to disturbances from a continuum of canopy structure and energy balance. This is a bi-directional gradient, resulting from deforestation and degradation in one direction, and forest regeneration or succession in the other. The characteristics of these disturbance gradients are integrally linked to canopy structural properties and may influence energy balance components and associated microclimates in linear or non-linear ways (Breshears, 2006; Stark et al., 2020). For example, as woody plant cover decreases, albedo and near-ground solar radiation increase, which increases the Bowen ratio (von Randow et al., 2004). Additionally, these patterns may also manifest nonlinearly, displaying threshold-type responses. Near-ground solar radiation, for instance, decreases nonlinearly with increasing CC. Similarly, surface roughness and associated wind flow category change nonlinearly with increasing cover (Breshears, 2006; Stark et al., 2020).

In this study we were only able to consider one ET date per season due to Landsat image availability. We acknowledge that this is insufficient for a full representation of the ET seasonal dynamics in our study area. We expect that current multi-spectral missions with improved spectral, temporal, and spatial resolutions will provide enough information on the seasonal characterization of ET and water stress in degraded forests in the Amazon. For instance, the ongoing ESA Sentinel mission with 10-m spatial resolution and 5-days revisit time (Berger et al., 2012) and future NASA Landsat NEXT with 10-m spatial resolution and 6-days revisit time (NGAC, 2018; Wu et al., 2019) are promising to the tracking of fast-changing ET dynamics.

### 4.2. Forest Structure Controls on Energy Balance

Although radiation controls on water and energy cycles prevail over our study area, forest structure seems to be an important secondary control of transpiration in degraded and secondary forests. Building on the Landsat-based ET and LST characterization during the dry season and the structural characterization provided by GEDI data, we showed that forest structure moderately explained ET and LST variability in the most heavily disturbed (burned and secondary) forests, whereas forest structure provided little or no ET and LST predictive power in the least disturbed logged and intact forests (Figure 8). These findings suggest that disturbances enhance ET biophysical controls (from forest structure) and that the contribution of canopy structural properties to ET and LST is modulated by disturbances and the associated water stress. Also, forest structure's contribution to ET decreased with time since disturbance, pointing to the functional recovery of these forests, with decreasing water stress and biophysical control over time as regeneration takes place.

Previous modeling studies converge with our findings. Using a land surface model, Mallick et al. (2016) quantified the controls on evaporation and transpiration across representative plant functional types in the Amazon and found enhanced biophysical influence on ET during the dry season, especially over pastures and dry forest functional types. This same effect was observed on the diurnal cycle, which shows higher VPD in the afternoon than in the morning, and during the strong 2005 drought. Longo et al. (2020) investigated the effects of forest degradation on ET using an ecosystem demography model and found that the magnitude and seasonality of fluxes were modulated by changes in forest structure caused by degradation. During the dry season and under typical conditions, severely degraded forests (biomass loss $\geq$66%) experienced water stress with declines in ET (up to 34%) and daily mean ground temperatures (up to 6.5°C) relative to intact forests.

Studies using observational data such as satellite observations and flux tower measurements also show degrees of agreement with our results. von Randow et al. (2012) found enhanced biophysical control on ET for pastures during the dry season, whereas the findings from Oliveira et al. (2019) suggested that the control of canopy stomatal conductance and root depth on vegetation water use is stronger in agricultural systems than in primary and secondary forests in the Amazon.

We observed larger ET and LST variability in the dry season for the majority of the forest classes (Figure 5). Hasler and Avissar (2007) also found a larger scatter of ET values during dry season throughout the Amazon and suggested that this effect is due to the increasing importance of secondary drivers of latent heat flux in the dry period, such as VPD and water availability. Our ESI annual profile (Figure 3) showing increasing evaporative stress toward the end of the dry season for all classes corroborates this. In contrast, the most recent classes (and likely, the most impacted) of logged, burned and secondary forests showed larger ET variability in the wet season (Figure 5), suggesting that these classes may be experiencing the dry season enhanced biophysical controls during the wet season as well. This hypothesis is also supported by the strong ET-LST relationships in these forests during both seasons (Figure 6).

Forest structure plays an essential role in determining roughness lengths and aerodynamic conductance to heat, moisture, and momentum between the canopy and the atmosphere (Bright et al., 2015). Supporting the strong influence of forest structure on the canopy and aerodynamic conductances, we found that ET and LST were strongly correlated with FHD, TCH, CC, and PAI (Table 3). Moreover, the FHD metric (an indirect measure of surface roughness given by structural complexity) was significantly lower in burned and secondary sites compared to intact forests (Figure 7) likely leading to decreased canopy conductance to heat and moisture and consequent lower ET and higher LST in these forests (Figures 5, Figure 6).

Due to their larger aerodynamic properties, forests are more efficient at dissipating sensible heat away from the surface and into the boundary layer relative to areas with shorter vegetation, particularly during the daytime (Bright et al., 2015; Hoffmann & Jackson, 2000). Our detailed characterization of ET, LST and forest structure relationships strongly supports these statements, as the classes with lower stature and complexity (depicted by CC and FHD metrics, Figure 7) showed the highest temperatures on both wet and dry seasons (Figure 5). Moreover, the highest correlation of the FHD metric with surface temperature also suggests that structural complexity plays an important role in cooling the canopy.

### 4.3. Implications for Vegetation Modeling

Land cover changes (Davidson et al., 2012) and their positive feedbacks in the precipitation variability in the Amazon Basin (Hilker et al., 2014; Wang et al., 2011) are expected to increase the canopy–atmosphere coupling of forest systems under drier conditions by altering the ratio of the biological and aerodynamic conductances. Our observational findings support previous model- and flux data-based findings showing that under drier conditions, the canopy-atmosphere coupling increases, and so the biophysical controls on ET amplify as well (de Oliveira et al., 2019; Longo et al., 2020; Restrepo-Coupe et al., 2013; von Randow et al., 2012). An increase in biophysical control is an indicator of a potential transpiration shift from an energy-limited to a water-limited regime due to the impact of air and surface temperatures and VPD on the canopy and aerodynamic conductance ratio (Mallick et al., 2016), with further consequences for the global surface water balance and rainfall recycling.

The implications of these findings to vegetation models in tropical forests are significant. The largely aggregated "big-leaf" vegetation models, which represent forests with single functional types, may not be able to characterize complex and heterogeneous structure-climate interactions across different forest types and disturbance conditions. Cohort-based vegetation models stand between "big leaf" and individual-based models and can efficiently represent structural and functional diversity within forest ecosystems at regional and global scales (Fisher et al., 2018). Cohort-based vegetation models may provide a more appropriate way to account for forest responses to the changes in the micro-environment caused by disturbances (Longo et al., 2020). Explicitly incorporating forest structure information into cohort-based vegetation models to inform about the degradation status and the degree of vegetation canopy coupling to the atmosphere could certainly improve estimates of seasonal water and energy fluxes at heterogeneous forests such as those in the Southern Amazon.

## Data Availability Statement

All the remote sensing data utilized in this study are freely available for users. MODIS and GEDI data can be accessed at the Land Processes Distributed Active Archive Center (LP DAAC—https://lpdaac.usgs.gov/). Landsat ET and LST data can be accessed at the EEFLUX page (http://eeflux-level1.appspot.com/). We uploaded the processed data with the corresponding metadata to a public repository available at Rangel Pinagé et al. (2023).

**Acknowledgments**

E. R. P. was supported by an Australian Government Research Training Program Scholarship, and by the USDA Forest Service Pacific Northwest Research Station and International Programs. The research carried out at the Jet Propulsion Laboratory, California Institute of Technology, was under a contract with the National Aeronautics and Space Administration (80NM0018D0004). M. L. was supported by the NASA Postdoctoral Program, administered by Universities Space Research Association under contract with NASA and the Next Generation Ecosystem Experiments-Tropics, funded by the U.S. Department of Energy, Office of Science, Office of Biological and Environmental Research (DE-AC02-05CH11231). Open access publishing facilitated by University of Technology Sydney, as part of the Wiley - University of Technology Sydney agreement via the Council of Australian University Librarians.

## References

Allen, R., Morton, C., Kamble, B., Kilic, A., Huntington, J., Thau, D., et al. (2015). EEFlux: A Landsat-based Evapotranspiration mapping tool on the Google Earth Engine. *ASABE / IA Irrigation Symposium: Emerging Technologies for Sustainable Irrigation St. Joseph, MI*.

Allen, R., Tasumi, M., & Trezza, R. (2007). Satellite-Based Energy Balance for Mapping Evapotranspiration with Internalized Calibration (METRIC) - model. *Journal of Irrigation and Drainage Engineering*, *133*(4), 380–394. https://doi.org/10.1061/(ASCE)0733-9437(2007)133:4(395)

Almeida, C. A. D., Coutinho, A. C., Esquerdo, J. C. D. M., Adami, M., Venturieri, A., Diniz, C. G., et al. (2016). High spatial resolution land use and land cover mapping of the Brazilian Legal Amazon in 2008 using Landsat-5/TM and MODIS data. *Acta Amazonica*, *46*(3), 291–302. https://doi.org/10.1590/1809-4392201505504

Anderson, M. C., Allen, R. G., Morse, A., & Kustas, W. P. (2012). Use of Landsat thermal imagery in monitoring evapotranspiration and managing water resources. *Remote Sensing of Environment*, *122*, 50–65. https://doi.org/10.1016/j.rse.2011.08.025

Arvor, D., Dubreuil, V., Ronchail, J., Simões, M., & Funatsu, B. M. (2014). Spatial patterns of rainfall regimes related to levels of double cropping agriculture systems in Mato Grosso (Brazil). *International Journal of Climatology*, *34*(8), 2622–2633. https://doi.org/10.1002/joc.3863

Barkhordarian, A., Saatchi, S. S., Behrangi, A., Loikith, P. C., & Mechoso, C. R. (2019). A recent systematic increase in vapor pressure deficit over tropical South America. *Scientific Reports*, *9*(1), 15331. https://doi.org/10.1038/s41598-019-51857-8

Bastiaanssen, W. G. M., Menenti, M., Feddes, R. A., & Holtslag, A. A. M. (1998). A remote sensing surface energy balance algorithm for land (SEBAL). 1. Formulation. *Journal of Hydrology*, *212–213*, 198–212. https://doi.org/10.1016/S0022-1694(98)00253-4

Berger, M., Moreno, J., Johannessen, J. A., Levelt, P. F., & Hanssen, R. F. (2012). ESA's sentinel missions in support of Earth system science. *Remote Sensing of Environment*, *120*, 84–90. https://doi.org/10.1016/j.rse.2011.07.023

Bonan, G. B. (2008). Forests and climate change: Forcings, feedbacks, and the climate benefits of forests. *Science*, *320*(5882), 1444–1449. https://doi.org/10.1126/science.1155121

Brando, P. M., Silvério, D., Maracahipes-Santos, L., Oliveira-Santos, C., Levick, S. R., Coe, M. T., et al. (2019). Prolonged tropical forest degradation due to compounding disturbances: Implications for $CO_2$ and $H_2O$ fluxes. *Global Change Biology*, *25*(9), 2855–2868. https://doi.org/10.1111/gcb.14659

Breshears, D. D. (2006). The grassland–forest continuum: Trends in ecosystem properties for woody plant mosaics? *Frontiers in Ecology and the environment*, (Vol. 4(2), pp. 96–104). https://doi.org/10.1890/1540-9295(2006)004[0096:TGCTIE]2.0.CO;2

Bright, R. M., Zhao, K., Jackson, R. B., & Cherubini, F. (2015). Quantifying surface albedo and other direct biogeophysical climate forcings of forestry activities. *Global Change Biology*, *21*(9), 3246–3266. https://doi.org/10.1111/gcb.12951

Brunsell, N. A., De Oliveira, G., Barlage, M., Shimabukuro, Y., Moraes, E., & Aragão, L. (2020). Examination of seasonal water and carbon dynamics in eastern Amazonia: A comparison of Noah-MP and MODIS. *Theoretical and Applied Climatology*, *143*(1–2), 571–586. https://doi.org/10.1007/s00704-020-03435-6

Chazdon, R. L. (2003). Tropical forest recovery: Legacies of human impact and natural disturbances. *Perspectives in Plant Ecology, Evolution and Systematics*, *6*(1), 51–71. https://doi.org/10.1078/1433-8319-00042

Coe, M., Macedo, M., Brando, P., Lefebvre, P., Panday, P., & Silvério, D. (2016). The hydrology and energy balance of the Amazon Basin. *Ecological Studies*, *227*, 35–53. https://doi.org/10.1007/978-3-662-49902-3_3

Costa, M. H., & Foley, J. A. (1997). Water balance of the Amazon Basin: Dependence on vegetation cover and canopy conductance. *Journal of Geophysical Research*, *102*(D20), 23973–23989. https://doi.org/10.1029/97jd01865

Csillik, O., Keller, M., Longo, M., Bonal, D., Burban, B., Chave, J., et al. (2022). Amazon forest structural diversity estimated using field inventory plots, airborne lidar and GEDI spaceborne lidar. *AGU Fall Meeting Abstracts*.

da Rocha, H. R., Manzi, A. O., Cabral, O. M., Miller, S. D., Goulden, M. L., Saleska, S. R., et al. (2009). Patterns of water and heat flux across a biome gradient from tropical forest to savanna in Brazil. *Journal of Geophysical Research*, *114*(G1). https://doi.org/10.1029/2007JG000640

Da Silva, P. E., Santos e Silva, C. M., Spyrides, M. H. C., & Andrade, L. d. M. B. (2019). Precipitation and air temperature extremes in the Amazon and northeast Brazil. *International Journal of Climatology*, *39*(2), 579–595. https://doi.org/10.1002/joc.5829

Davidson, E. A., de Araújo, A. C., Artaxo, P., Balch, J. K., Brown, I. F., Bustamante, M. M., et al. (2012). The Amazon basin in transition. *Nature*, *481*(7381), 321–328. https://doi.org/10.1038/nature10717

de Oliveira, G., Brunsell, N. A., Moraes, E. C., Shimabukuro, Y. E., dos Santos, T. V., von Randow, C., et al. (2019). Effects of land-cover changes on the partitioning of surface energy and water fluxes in Amazonia using high-resolution satellite imagery. *Ecohydrology*, *12*(6), e2126. https://doi.org/10.1002/eco.2126

Diniz, C. G., Souza, A. A. d. A., Santos, D. C., Dias, M. C., Luz, N. C. d., Moraes, D. R. V. d., et al. (2015). DETER-B: The new Amazon near real-time deforestation detection system. *IEEE Journal of Selected Topics in Applied Earth Observations and Remote Sensing*, *8*(7), 3619–3628. https://doi.org/10.1109/JSTARS.2015.2437075

Dubayah, R., Armston, J., Healey, S. P., Bruening, J. M., Patterson, P. L., Kellner, J. R., et al. (2022). GEDI launches a new era of biomass inference from space. *Environmental Research Letters*, *17*(9), 095001. https://doi.org/10.1088/1748-9326/ac8694

Dubayah, R., Blair, J. B., Goetz, S., Fatoyinbo, L., Hansen, M., Healey, S., et al. (2020). The global ecosystem dynamics investigation: High-resolution laser ranging of the Earth's forests and topography. *Science of Remote Sensing*, *1*, 100002. https://doi.org/10.1016/j.srs.2020.100002

Duncanson, L., Kellner, J. R., Armston, J., Dubayah, R., Minor, D. M., Hancock, S., et al. (2022). Aboveground biomass density models for NASA's Global Ecosystem Dynamics Investigation (GEDI) lidar mission. *Remote Sensing of Environment*, *270*, 112845. https://doi.org/10.1016/j.rse.2021.112845

Fisher, J. B. (2013). Land-atmosphere interactions, evapotranspiration. In E. G. Njoku (Ed.), *Encyclopedia of remote sensing* (pp. 1–5). Springer-Verlag.

Fisher, J. B., Malhi, Y., Bonal, D., da Rocha, H. R., de Araujo, C. A., Gamo, M., et al. (2009). The land–atmosphere water flux in the tropics. *Global Change Biology*, *15*(11), 2694–2714. https://doi.org/10.1111/j.1365-2486.2008.01813.x

Fisher, J. B., Melton, F., Middleton, E., Hain, C., Anderson, M., Allen, R., et al. (2017). The future of evapotranspiration: Global requirements for ecosystem functioning, carbon and climate feedbacks, agricultural management, and water resources. *Water Resources Research*, *53*(4), 2618–2626. https://doi.org/10.1002/2016wr020175

Fisher, J. B., Tu, K. P., & Baldocchi, D. D. (2008). Global estimates of the land–atmosphere water flux based on monthly AVHRR and ISLSCP-II data, validated at 16 FLUXNET sites. *Remote Sensing of Environment*, *112*(3), 901–919. https://doi.org/10.1016/j.rse.2007.06.025

Fisher, R. A., Koven, C. D., Anderegg, W. R. L., Christoffersen, B. O., Dietze, M. C., Farrior, C. E., et al. (2018). Vegetation demographics in Earth system models: A review of progress and priorities. *Global Change Biology*, *24*(1), 35–54. https://doi.org/10.1111/gcb.13910

Hasler, N., & Avissar, R. (2007). What controls evapotranspiration in the Amazon Basin? *Journal of Hydrometeorology*, *8*(3), 380–395. https://doi.org/10.1175/jhm587.1

Hilker, T., Lyapustin, A. I., Tucker, C. J., Hall, F. G., Myneni, R. B., Wang, Y., et al. (2014). Vegetation dynamics and rainfall sensitivity of the Amazon. *Proceedings of the National Academy of Sciences*, *111*(45), 16041–16046. https://doi.org/10.1073/pnas.1404870111

Hoffmann, W. A., & Jackson, R. B. (2000). Vegetation–climate feedbacks in the conversion of tropical savanna to grassland. *Journal of Climate*, *13*(9), 1593–1602. https://doi.org/10.1175/1520-0442(2000)013<1593:Vcfitc>2.0.Co;2

Hofton, M., Blair, J. B., Story, S., & Yi, D. (2019). Algorithm Theoretical Basis Document (ATBD) for GEDI transmit and receive waveform processing for L1 and L2 products V. 1.0.

Huang, M., Xu, Y., Longo, M., Keller, M., Knox, R. G., Koven, C. D., & Fisher, R. A. (2020). Assessing impacts of selective logging on water, energy, and carbon budgets and ecosystem dynamics in Amazon forests using the Functionally Assembled Terrestrial Ecosystem Simulator. *Biogeosciences*, *17*(20), 4999–5023. https://doi.org/10.5194/bg-17-4999-2020

IBGE. (2021). Mapeamento de Recursos Naturais do Brasil - Escala 1:250.000 - Versão 2021 version 2021). Retrieved from https://www.ibge.gov.br/geociencias/informacoes-ambientais/vegetacao/22453-cartas-1-250-000.html?=&t=downloads

INPE. (2020). PRODES - Monitoramento da Floresta Amazônica por Satélite. In *São josé dos Campos*. National Institute for Space Research.
Jarvis, P. G., & McNaughton, K. G. (1986). Stomatal control of transpiration: Scaling up from leaf to region. In A. MacFadyen & E. D. Ford (Eds.), *Advances in Ecological research* (Vol. 15, pp. 1–49). Academic Press. https://doi.org/10.1016/S0065-2504(08)60119-1
Jucker, T., Hardwick, S. R., Both, S., Elias, D. M. O., Ewers, R. M., Milodowski, D. T., et al. (2018). Canopy structure and topography jointly constrain the microclimate of human-modified tropical landscapes. *Global Change Biology*, *24*(11), 5243–5258. https://doi.org/10.1111/gcb.14415
Lathuillière, M. J., Johnson, M. S., & Donner, S. D. (2012). Water use by terrestrial ecosystems: Temporal variability in rainforest and agricultural contributions to evapotranspiration in Mato Grosso, Brazil. *Environmental Research Letters*, *7*(2), 024024. https://doi.org/10.1088/1748-9326/7/2/024024
Lefsky, M., Cohen, W. B., Parker, G., & Harding, D. J. (2002). Lidar remote sensing for ecosystem studies. *BioScience*, *52*(1), 19–30. https://doi.org/10.1641/0006-3568(2002)052[0019:lrsfes]2.0.co;2
Longo, M., Saatchi, S., Keller, M., Bowman, K., Ferraz, A., Moorcroft, P. R., et al. (2020). Impacts of degradation on water, energy, and carbon cycling of the Amazon tropical forests. *Journal of Geophysical Research: Biogeosciences*, *125*(8), e2020JG005677. https://doi.org/10.1029/2020JG005677
Maeda, E., Ma, X., Wagner, F., Kim, H., Oki, T., Eamus, D., & Huete, A. (2017). Evapotranspiration seasonality across the Amazon Basin. *Earth System Dynamics*, *8*(2), 439–454. https://doi.org/10.5194/esd-8-439-2017
Malhi, Y., Pegoraro, E., Nobre, A. D., Pereira, M. G., Grace, J., Culf, A. D., & Clement, R. (2002). Energy and water dynamics of a central Amazonian rain forest. *Journal of Geophysical Research*, *107*(D20), 8061. https://doi.org/10.1029/2001jd000623
Mallick, K., Trebs, I., Boegh, E., Giustarini, L., Schlerf, M., Drewry, D. T., et al. (2016). Canopy-scale biophysical controls of transpiration and evaporation in the Amazon Basin. *Hydrology and Earth System Sciences*, *20*(10), 4237–4264. https://doi.org/10.5194/hess-20-4237-2016
MapBiomas Project. (2019). Collection 45.0 of the annual series of land use and land cover maps of Brazil. Retrieved from https://mapbiomas.org/en
Matricardi, E. A., Skole, D. L., Pedlowski, M. A., Chomentowski, W., & Fernandes, L. C. (2010). Assessment of tropical forest degradation by selective logging and fire using Landsat imagery. *Remote Sensing of Environment*, *114*(5), 1117–1129. https://doi.org/10.1016/j.rse.2010.01.001
Miller, S. D., Goulden, M. L., Hutyra, L. R., Keller, M., Saleska, S. R., Wofsy, S. C., et al. (2011). Reduced impact logging minimally alters tropical rainforest carbon and energy exchange. *Proceedings of the National Academy of Sciences*, *108*(48), 19431–19435. https://doi.org/10.1073/pnas.1105068108
Morton, D., Le Page, Y., DeFries, R., Collatz, G., & Hurtt, G. (2013). Understorey fire frequency and the fate of burned forests in southern Amazonia. *Philosophical Transactions of the Royal Society B: Biological Sciences*, *368*(1619), 20120163. https://doi.org/10.1098/rstb.2012.0163
Mu, Q., Zhao, M., & Running, S. W. (2011). Improvements to a MODIS global terrestrial evapotranspiration algorithm. *Remote Sensing of Environment*, *115*(8), 1781–1800. https://doi.org/10.1016/j.rse.2011.02.019
Nepstad, D. C., de Carvalho, C. R., Davidson, E. A., Jipp, P. H., Lefebvre, P. A., Negreiros, G. H., et al. (1994). The role of deep roots in the hydrological and carbon cycles of Amazonian forests and pastures. *Nature*, *372*(6507), 666–669. https://doi.org/10.1038/372666a0
NGAC. (2018). National Geospatial Advisory Committee. *Recommendations for possible future U.S. Global Land Data Collection Missions Beyond Landsat 9: A report of the National Geospatial Advisory Committee Landsat Advisory Group*. Retrieved from https://www.fgdc.gov/ngac/meetings/april-2018/ngac-landsat-future-missions-recommendations-paper.pdf
Numata, I., Khand, K., Kjaersgaard, J., Cochrane, M. A., & Silva, S. S. (2017). Evaluation of Landsat-based METRIC modeling to provide high-spatial resolution evapotranspiration estimates for Amazonian forests. *Remote Sensing*, *9*(1), 46. https://doi.org/10.3390/rs9010046
O'Connor, J., Santos, M. J., Rebel, K. T., & Dekker, S. C. (2019). The influence of water table depth on evapotranspiration in the Amazon arc of deforestation. *Hydrology and Earth System Sciences*, *23*(9), 3917–3931. https://doi.org/10.5194/hess-23-3917-2019
Oliveira, G., Brunsell, N. A., Moraes, E. C., Shimabukuro, Y. E., Santos, T. V., Randow, C., et al. (2019). Effects of land-cover changes on the partitioning of surface energy and water fluxes in Amazonia using high-resolution satellite imagery. *Ecohydrology*, *12*(6), e2126. https://doi.org/10.1002/eco.2126
Rangel Pinagé, E., Bell, D. M., Longo, M., Silva, C. A., Csillik, O., & Huete, A. (2023). Supporting dataset for "Surface energy dynamics and canopy structural properties in intact and disturbed forests in the Southern Amazon. (Version 1) [Dataset]. https://doi.org/10.5281/zenodo.8021957
Rangel Pinagé, E., Bell, D. M., Longo, M., Gao, S., Keller, M., Silva, C. M., et al. (2022). Forest structure and solar-induced fluorescence across intact and degraded forests in the Amazon. *Remote Sensing of Environment*, *274*, 112998. https://doi.org/10.1016/j.rse.2022.112998
R Core Team. (2021). R: A Language and environment for statistical computing. In *R foundation for statistical computing*. Retrieved from https://www.R-project.org/
Restrepo-Coupe, N., da Rocha, H. R., Hutyra, L. R., da Araujo, A. C., Borma, L. S., Christoffersen, B., et al. (2013). What drives the seasonality of photosynthesis across the Amazon basin? A cross-site analysis of eddy flux tower measurements from the Brasil flux network. *Agricultural and Forest Meteorology*, *182*, 128–144. https://doi.org/10.1016/j.agrformet.2013.04.031
Running, S. W., Mu, Q., & Zhao, M. (2017). MYD16A2 MODIS/Aqua net evapotranspiration 8-day L4 global 500m SIN grid V006. https://doi.org/10.5067/MODIS/MYD16A2.006
Silva, C. A., Hamamura, C., Valbuena, R., Hancock, S., Cardil, A., Broadbent, E. N., et al. (2020). rGEDI: NASA's Global Ecosystem Dynamics Investigation (GEDI) data visualization and processing. R package version 0.1.7. Retrieved from https://CRAN.R-project.org/package=rGEDI
Silvério, D. V., Brando, P. M., Macedo, M. N., Beck, P. S. A., Bustamante, M., & Coe, M. T. (2015). Agricultural expansion dominates climate changes in southeastern Amazonia: The overlooked non-GHG forcing. *Environmental Research Letters*, *10*(10), 104015. https://doi.org/10.1088/1748-9326/10/10/104015
Souza, C. M., Roberts, D. A., & Cochrane, M. A. (2005). Combining spectral and spatial information to map canopy damage from selective logging and forest fires. *Remote Sensing of Environment*, *98*(2), 329–343. https://doi.org/10.1016/j.rse.2005.07.013
Spracklen, D. V., Arnold, S. R., & Taylor, C. M. (2012). Observations of increased tropical rainfall preceded by air passage over forests. *Nature*, *489*(7415), 282–285. https://doi.org/10.1038/nature11390
Spracklen, D. V., Baker, J. C. A., Garcia-Carreras, L., & Marsham, J. H. (2018). The effects of tropical vegetation on rainfall. *Annual Review of Environment and Resources*, *43*(1), 193–218. https://doi.org/10.1146/annurev-environ-102017-030136
Stark, S. C., Breshears, D. D., Aragón, S., Villegas, J. C., Law, D. J., Smith, M. N., et al. (2020). Reframing tropical savannization: Linking changes in canopy structure to energy balance alterations that impact climate. *Ecosphere*, *11*(9), e03231. https://doi.org/10.1002/ecs2.3231
Tang, H., & Armston, J. (2019). Algorithm Theoretical Basis Document (ATBD) for GEDI L2B footprint canopy cover and vertical profile metrics. Retrieved from Retrieved from https://lpdaac.usgs.gov/documents/588/GEDI_FCCVPM_ATBD_v1.0.pdf
Tukey, J. W. (1977). Exploratory Data Analysis (Vol. *2*).

van der Ent, R. J., Savenije, H. H. G., Schaefli, B., & Steele-Dunne, S. C. (2010). Origin and fate of atmospheric moisture over continents. *Water Resources Research*, *46*(9). https://doi.org/10.1029/2010wr009127

von Randow, C., Manzi, A. O., Kruijt, B., de Oliveira, P. J., Zanchi, F. B., Silva, R. L., et al. (2004). Comparative measurements and seasonal variations in energy and carbon exchange over forest and pasture in South West Amazonia. *Theoretical and Applied Climatology*, *78*(1), 5–26. https://doi.org/10.1007/s00704-004-0041-z

von Randow, R. C. S., von Randow, C., Hutjes, R. W. A., Tomasella, J., & Kruijt, B. (2012). Evapotranspiration of deforested areas in central and southwestern Amazonia. *Theoretical and Applied Climatology*, *109*(1), 205–220. https://doi.org/10.1007/s00704-011-0570-1

Von Randow, R. D. C. S., Tomasella, J., Von Randow, C., De Araújo, A. C., Manzi, A. O., Hutjes, R., & Kruijt, B. (2020). Evapotranspiration and gross primary productivity of secondary vegetation in Amazonia inferred by eddy covariance. *Agricultural and Forest Meteorology*, *294*, 108141. https://doi.org/10.1016/j.agrformet.2020.108141

Vourlitis, G. L., de Souza Nogueira, J., de Almeida Lobo, F., Sendall, K. M., de Paulo, S. R., Antunes Dias, C. A., et al. (2008). Energy balance and canopy conductance of a tropical semi-deciduous forest of the southern Amazon Basin. *Water Resources Research*, *44*(3). https://doi.org/10.1029/2006WR005526

Wang, G., Sun, S., & Mei, R. (2011). Vegetation dynamics contributes to the multi-decadal variability of precipitation in the Amazon region. *Geophysical Research Letters*, *38*(19). https://doi.org/10.1029/2011GL049017

Wu, Z., Snyder, G., Vadnais, C., Arora, R., Babcock, M., Stensaas, G., et al. (2019). User needs for future Landsat missions. *Remote Sensing of Environment*, *231*, 111214. https://doi.org/10.1016/j.rse.2019.111214

Wulder, M. A., Loveland, T. R., Roy, D. P., Crawford, C. J., Masek, J. G., Woodcock, C. E., et al. (2019). Current status of Landsat program, science, and applications. *Remote Sensing of Environment*, *225*, 127–147. https://doi.org/10.1016/j.rse.2019.02.015

Zemp, D. C., Schleussner, C.-F., Barbosa, H. M. J., Hirota, M., Montade, V., Sampaio, G., et al. (2017). Self-amplified Amazon forest loss due to vegetation-atmosphere feedbacks. *Nature Communications*, *8*(1), 14681. https://doi.org/10.1038/ncomms14681